Evaluation of the ^{182}Ta radiative strength function via χ^2-weighted model averaging

Nguyen Hoang Phuc[1], Phan Bao Quoc Hieu[1], Dinh Tien Hung[2], Le Tan Phuc[3, 4], Nguyen Ngoc Anh[5*]

[1]Dalat Nuclear Research Institute, 1 Nguyen Tu Luc, Lam Vien - Da Lat, Lam Dong, Vietnam;
[2]The Military Institute of Chemical and Environmental Engineering (MICEE), CT03, An Khanh, Hanoi, Vietnam;
[3]Institute of Fundamental and Applied Sciences, Duy Tan University, 6 Tran Nhat Duat, Tan Dinh, Ho Chi Minh City, Vietnam;
[4]Faculty of Natural Sciences, Duy Tan University, 254 Nguyen Van Linh, Danang, Vietnam;
[5]Phenikaa Institute for Advanced Study (PIAS), Phenikaa University, Nguyen Trac, Duong Noi, Hanoi, Vietnam.
[*]Corresponding author: anh.nguyenngoc1@phenikaa-uni.edu.vn
Received 14 Feb. 2026; Revised 24 Apr. 2026; Accepted 11 May 2026; Published 25 May 2026.
DOI: https://doi.org/10.54939/1859-1043.j.mst.111.2026.104-111

ABSTRACT

Determining the radiative strength function (RSF) for ^{182}Ta is currently hindered by fragmented experimental coverage, leaving significant discrepancies between theoretical models, especially in the regions where experimental data are unavailable. This work addresses this gap by evaluating an ensemble of 78 E1 and M1 model combinations using a χ^2-weighted averaging method constrained by total experimental strength data from the Oslo method. Among the models tested, the Hartree-Fock-Bogoliubov plus quasiparticle random phase approximation with the D1M Gogny force framework exhibits the highest consistency with experimental observations. This is followed by the microscopic exact pairing plus phonon-damping model. In general, our results demonstrate that this data-driven weighting significantly reduces theoretical variance.

Keywords: Radiative strength function; ^{182}Ta; χ^2-weighted model.

1. INTRODUCTION

The radiative strength function (RSF) is a critical statistical property of atomic nuclei, describing their electromagnetic transition probabilities [1]. In the context of the Hauser-Feshbach statistical model [2], the RSF is an essential input for calculating capture cross-sections, such as the (n, γ) reactions [3]. These cross-sections are fundamental for modeling the nucleosynthesis of heavy elements in astrophysical environments [4, 5] and for various applications in nuclear engineering and medical physics.

The accurate determination of the RSF for ^{182}Ta is essential across diverse fields, ranging from nuclear engineering and astrophysics to medical physics. As a cornerstone material in fast neutron reactors, accelerator-driven systems, and future fusion technologies, Tantalum's neutron capture cross-sections are vital for calculating fuel burnup and operational safety [6, 7]. Furthermore, the ^{182}Ta isotope serves as a critical calibration standard for γ-ray spectrometry [8, 9] and a significant therapeutic agent in interstitial brachytherapy [10], while also acting as a key component in the nucleosynthetic s-process within the Ta-W mass region [11].

Due to the critical importance of ^{182}Ta, various experimental campaigns have been conducted to map its RSF. For the electric dipole (*E1*) RSF, data are primarily available from photo-neutron (γ, n) cross-section measurements [12-14], which accurately describe the giant dipole resonance (GDR) region at high energies ($E_\gamma \geq 10$ MeV). At lower energies, average resonance capture (ARC) [15] and discrete resonance capture (DRC) [16] provide localized data points near the neutron separation energy (S_n). Similarly, the magnetic dipole (*M1*) RSF has been investigated through resonance capture, namely ARC and DRC [15, 16].

However, a significant limitation persists: these experimental techniques cover only fragmented portions of the energy spectrum. While (γ, n) data characterize the high-energy behavior, they provide no information below the S_n threshold. Conversely, resonance capture data offer high precision but are restricted to a very narrow energy window. This lack of continuous coverage necessitates the use of theoretical models to interpolate and extrapolate the strength functions across the full energy range required for Hauser-Feshbach calculations. We observe that while theoretical predictions generally converge within the regions constrained by experimental data, they tend to vary significantly in the energy gaps where no empirical measurements exist. Consequently, it is necessary to reduce the uncertainty of these theoretical predictions.

Fortunately, recent experimental data showing the summed *E1* + *M1* strength, obtained using the Oslo method via ^{182}Ta (*d*,*X*) and ^{181}Ta(^{3}He,*X*) reactions [17], can be used as a further constraint to bridge these gaps and improve the reliability of model extrapolations. In this work, we evaluate various theoretical models by comparing their total (*E1* + *M1*) predictions against the Oslo data. By calculating the χ^2 for each model, we determine a weighted average that prioritizes the models with the best fit to the experimental results. A detailed breakdown of this methodology is provided in Section 2.

2. EVALUATION METHOD

In this work, we address the challenge of theoretical uncertainty by compiling a comprehensive set of model combinations that satisfy experimental constraints for both *E1* and *M1* components. We calculate the total photon strength function, $f_{tot} = f_{E1} + f_{M1}$, for each model pair and perform a direct comparison with the Oslo data [17], resulting in a χ^2 value corresponding to each model pair. The final evaluated RSFs, including *E1*, *M1*, and *E1*+*M1*, are determined using a weighted average, where the statistical weight for each pair is defined as $1/\chi^2$.

We consider a variety of theoretical approaches to describe the dipole strength. The models for the *E1* component are illustrated in Figure 1, and the models for the *M1* component are shown in Figure 2. It can be seen that the selected models all well describe the available experimental *E1* and *M1* RSFs. However, they show significant discrepancies in energy regions where experimental data are unavailable. For *E1* RSF, the selected models are: Generalized Lorentzian (GLO) [18], Standard Lorentzian (SLO) [19], Hartree-Fock-Bogoliubov plus Quasiparticle random phase approximation (QRPA) (HFB) [20], Skyrme Hartree-Fock plus Bardeen-Cooper-Schrieffer and QRPA (HFBCS) [21], Goriely's hybrid [22], Goriely's Hartree-Fock-Bogoliubov plus QRPA at finite temperature (Goriely's HFBT) [20], Temperature-dependent relativistic HFB mean-field plus QRPA (T-dependent RMF) [23], Triple Lorentzian (TLO) [24], Exact Pairing plus Phonon Damping model [EP+PDM] [25], Simplified modified Lorentzian (SMLO) [26], and HFB plus QRPA with D1M Gogny force (D1M) [27]. The last three models are also considered for *M1* RSF together with the spin flip (SF) one [18]. It should be noted that for temperature-dependent *RSF* models, each specific temperature setting is treated as a distinct, individual model within our ensemble. These temperatures are chosen to be as close as possible to the values provided in the systematic evaluation given in Ref. [28] for ^{182}Ta nucleus, namely 0.57 MeV. For the EP+PDM, we adopt the temperature value consistent with the original work, namely 0.7 MeV.

The selection of the models in the present work is motivated by their widespread reliability and theoretical diversity. We include the standard models implemented in TALYS [3], as it is the most widely utilized nuclear reaction code in the field. To ensure our evaluation is grounded in experimentally validated benchmarks, we adopt the models provided by the IAEA RSF database [29], which aggregates and evaluates theoretical RSFs against all available experimental sources. Furthermore, the microscopic EP+PDM is included due to its demonstrated predictive potential.

In a previous study, the EP+PDM framework, when coupled with the Exact Pairing plus

Independent Particle model for the nuclear level density, has predicted Maxwellian-averaged cross sections in good agreement with experimental data, then expressing its impact in studying the interesting $^{182}W/^{184}W$ ratio in nuclear astrophysics. However, while these earlier results established a strong visual and qualitative correspondence, they did not provide a rigorous metric for performance relative to the wide array of other established theoretical models. In the present work, the EP+PDM is treated on the same footing as the other candidates within our ensemble. This allows us to move beyond visual comparison and provide a rigorous quantitative assessment of the model's performance.

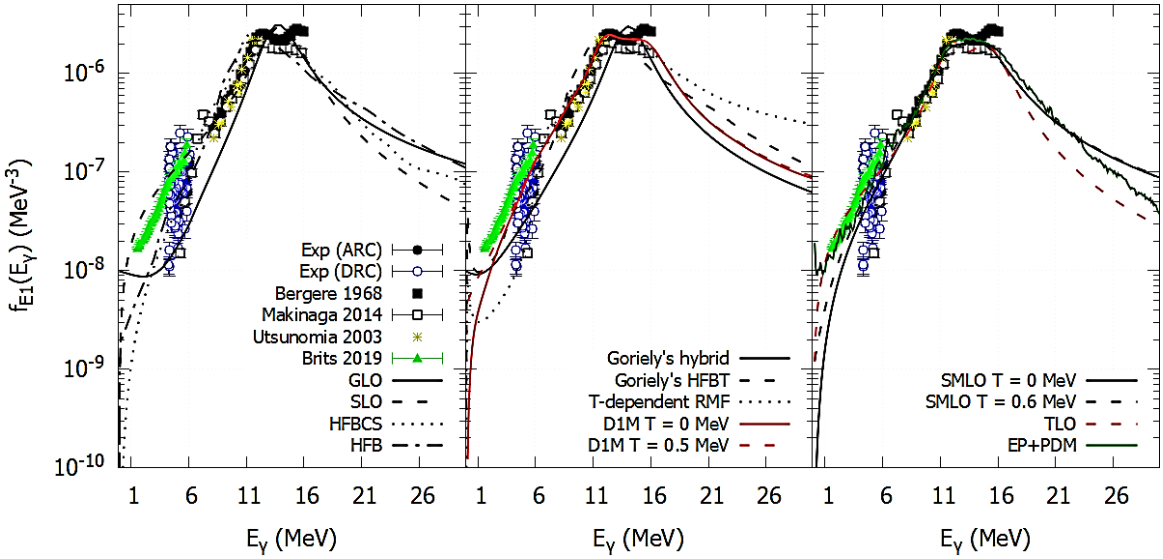

Figure 1. *Experimental and theoretical electric dipole (E1) radiative strength functions (f_{E1}) for ^{182}Ta. Experimental data are taken from Oslo method (Brits 2019) [17], ARC [15] and DRC [16] methods, as well as from (γ,n) reactions (Bergere 1968 [12], Makinaga 2014 [13], and Utsunomiya 2003 [14]). Curves represent the various theoretical models discussed in the text. For clarity, the comparison is divided into three separate panels.*

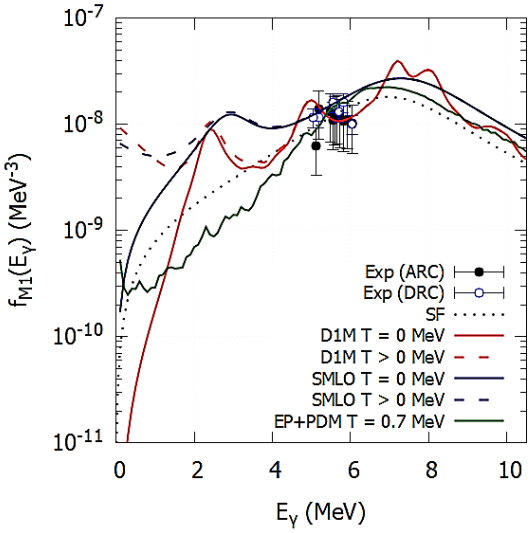

Figure 2. *Experimental and theoretical magnetic dipole (M1) radiative strength functions (f_{M1}) for ^{182}Ta. Experimental data are taken from ARC [15] and DRC [16] methods. Curves represent the various theoretical models discussed in the text.*

In total, there are thirteen *E1* and six *M1* RSF models involved in the present evaluation, making 78 model pairs/combinations for the total *E1+M1* RSF. The theoretical RSFs used in this analysis are taken in their tabulated forms from established libraries, specifically the TALYS internal library [3], the IAEA RSF database [29]. The EP+PDM RSFs are an exception, as they were obtained directly from the authors of the original study [25]. By utilizing these pre-calculated data, we avoid the complexity of full-scale theoretical derivations, which is not the primary focus of the present work.

We define the total theoretical RSF for any given combination *k* of an *E1* model (*i*) and an *M1* model (*j*) as $f_{cal,k} = f_{E1,i} + f_{M1,j}$. To assess the quality of these combinations, we calculate the χ^2 value relative to the experimental Oslo data [17], bearing in mind that this experimental data set represents the summation of *E1* and *M1* RSF of ^{182}Ta:

$$\chi_k^2 = \frac{1}{N}\sum_{p=1}^{N}\left[\frac{f_{exp}(E_p) - f_{calc,k}(E_p)}{\sigma_{exp}(E_p)}\right]^2 \quad (1)$$

where *N* is the number of experimental data points, f_{exp} is the Oslo data and σ_{exp} is the associated experimental uncertainty. Instead of selecting a single best model, we perform a weighted average to account for the inherent model dependencies. The weighted mean RSF, $\bar{f}$, is calculated as:

$$\bar{f}(E_\gamma) = \frac{\sum_k f_k(E_\gamma) \times w_k}{\sum_k w_k} \quad (2)$$

In this evaluation, we use $w_k = 1/\chi^2$. This ensures that model combinations providing a better fit to the experimental total strength contribute more significantly to the final recommended value. To represent the model-dependent uncertainty, we calculate the weighted standard deviation. This value characterizes the spread of the theoretical predictions constrained by the experimental data, i.e.

$$\Delta\bar{f}(E) = \sqrt{\frac{\sum_k w_k f_k^2(E)}{\sum_k w_k} - \left[\bar{f}(E)\right]^2} \quad (3)$$

3. RESULTS AND DISCUSSION

Figures 1 and 2 clearly illustrate the experimental fragmentation discussed above (see the Introduction section). The (γ,n) data define the GDR region but provide no information below the S_n threshold, while resonance capture data are restricted to a very narrow energy window, i.e., approximately from 4.5 to 5.5 MeV. This lack of continuous coverage necessitates model-based interpolation, where we observe significant theoretical divergence in the data-poor gaps. In Figure 1, the total Oslo RSF data ($f_{E1} + f_{M1}$) are provided as a benchmark. As anticipated, the majority of $E1$ models fall below the total Oslo strength. However, the SLO and TLO models are notable exceptions, as they both overestimate the Oslo data in the low-energy region. For the $M1$ RSF shown in Figure 2, there is a substantial fluctuation at low energies. This is due to the inclusion of phenomenological terms in the D1M and SMLO models, specifically targeting the low-energy enhancement (LEE) and the scissors resonance (SR). The resulting variance underscores the necessity of our χ^2-weighted averaging approach to reconcile these divergent predictions with the total available experimental strength.

The results of our χ^2 evaluation are summarized in Figure 3. As shown in Figure 3a, the constraint provided by the Oslo data significantly reduces the uncertainty of the model predictions. Even when considering the full ensemble without a specific threshold (the blue shaded band), the uncertainty is notably lower compared to the raw variance of all individual theoretical models (represented by the gray lines). This uncertainty is further suppressed as the χ^2 threshold is tightened to 50.0 (green band) and 16.6 (red band). However, we observe that the top-performing

models still tend to slightly underestimate the Oslo data in the higher energy region of the spectrum. This may stem from two primary factors. First, it suggests a potential lack of small resonance structures, such as minor collective modes, which are not explicitly parameterized in the theoretical models included in our ensemble. Second, while our model combinations are restricted to the summation of $E1$ and $M1$ components, higher multipolarity transitions, such as $E2$ ones, might contribute to the total strength captured in the experimental Oslo data. Consequently, further dedicated studies and more detailed theoretical refinements will be conducted in the future to clarify these localized contributions and enhance the predictive accuracy of the radiative strength function in this energy region.

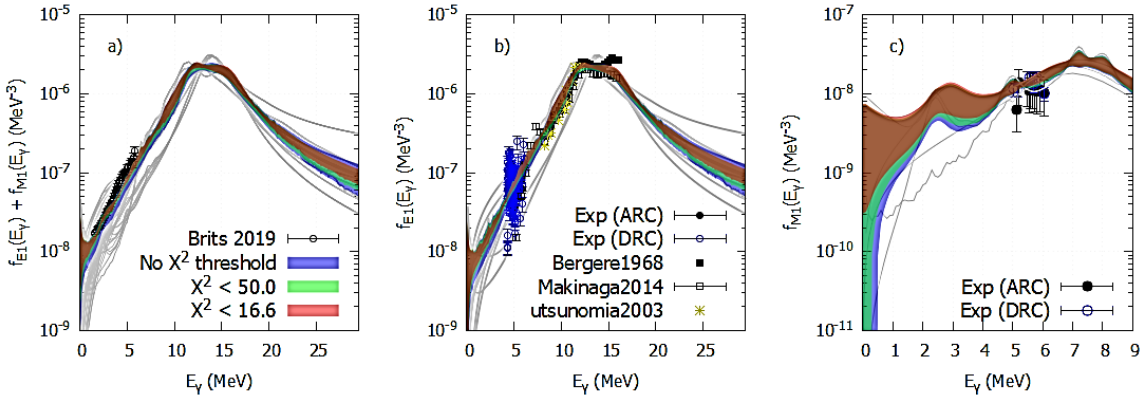

Figure 3. *Evaluation of the ^{182}Ta radiative strength function using χ^2-weighted averaging: (a) Total RSF ($f_{E1} + f_{M1}$) compared with experimental Oslo data (Brits 2019) [17]; b) E1 RSF (f_{E1}) compared with ARC, DRC, and (γ,n) experimental data [12-16]; and c) M1 RSF (f_{M1}) compared with the ARC and DRC experimental data [15, 16]. Shaded bands represent results obtained with the model ensemble with no threshold (blue), $\chi^2 < 50.0$ (green), and $\chi^2 < 16.6$ (red). Gray lines represent the variant corresponding to the predictions of all the theoretical models involved.*

Figures 3b and 3c illustrate the reduction in uncertainty for the individual *E1* and *M1* components, respectively. While the *E1* component is well-constrained, the *M1* uncertainty remains relatively large, particularly in the low-energy region below 2 MeV. This suggests that the total strength data, while restrictive, still allows for some ambiguity in the magnitude of the *M1* in the low-energy region. The enhancement tail observed in this region (see Figures 2 and 3c) originates from the fact that both the SMLO and D1M models incorporate specific phenomenological terms to describe low-energy magnetic features, i.e., the LEE and SR mentioned above. The LEE term is implemented to account for the observed increase in dipole strength as the gamma energy approaches zero, a feature often attributed to $M1$ transitions between closely spaced states in the quasi-continuum. Meanwhile, the scissors mode represents a collective magnetic excitation associated with the relative oscillation of protons against neutrons in deformed nuclei. Since these features are parameterized phenomenologically within SMLO and D1M, their varying magnitudes across different models contribute to the wide theoretical spread seen in Figures 2 and 3c, indicating that the total experimental strength alone cannot yet fully resolve the individual contributions of these magnetic modes. Therefore, obtaining high-precision experimental $M1$ data remains vital for future studies to disentangle these localized contributions.

The ten model combinations that yielded the best agreement with the experimental data are listed in Table 1. A key observation is the prominent role of the D1M model (based on the Gogny interaction) in the description of ^{182}Ta. Specifically, the D1M (T=0.5 MeV), which incorporates temperature effects, appears in the majority of the top-performing combinations. This indicates that the D1M framework, when evaluated at temperatures consistent with the systematic evaluation in Ref. [28], provides a superior description of the *E1* strength for this isotope.

The results summarized in Table 1 also highlight the competitive performance of the EP+PDM, which appears twice among the top ten combinations. Notably, the rank-7 combination consisting of both EP+PDM $E1$ and $M1$ components, strengthens the selection of EP+PDM, which was based on a visual comparison, in the study of Maxwellian-averaged cross-section [25]. A significant observation is the discrepancy in the optimal temperature between the leading models. While the D1M framework favors $T = 0.5$ MeV, the EP+PDM performs best at $T = 0.7$ MeV. Theoretically, D1M and SMLO incorporate the temperature dependence of the gamma width using an infinite Fermi liquid approximation. Conversely, the EP+PDM calculates these effects microscopically based on the couplings of PDM phonons with particle and hole states. Although the infinite Fermi liquid approach is theoretically optimized for the high-temperature limit, the present χ^2 evaluation indicates that it provides a superior description of the experimental data for ^{182}Ta. This finding suggests that the precise nature of temperature dependence in RSF remains an open question, and the temperature settings for these microscopic models warrant further systematic investigation.

Table 1. *Top ten theoretical model combinations for ^{182}Ta ranked by their χ^2 agreement with Oslo data.*

Rank	*M1* Model	*E1* Model	χ^2
1	SMLO (*T>0 MeV*)	D1M (*T=0.5 MeV*)	5.319
2	SMLO (*T=0 MeV*)	D1M (*T=0.5 MeV*)	5.594
3	D1M (*T>0 MeV*)	D1M (*T=0.5 MeV*)	8.487
4	SF	EP+PDM (*T=0.7 MeV*)	10.100
5	SMLO (*T>0 MeV*)	Goriely's HFBT	10.483
6	SMLO (*T>0 MeV*)	SMLO (*T=0.6 MeV*)	11.465
7	EP+PDM (*T=0.7 MeV*)	EP+PDM (*T=0.7 MeV*)	14.110
8	D1M (*T=0 MeV*)	D1M (*T=0.5 MeV*)	14.882
9	SMLO (*T=0 MeV*)	Goriely's HFBT	15.098
10	SMLO (*T>0 MeV*)	D1M (*T=0 MeV*)	16.580

4. CONCLUSIONS

This study evaluates the radiative strength function (RSF) for ^{182}Ta by applying a χ^2-weighted averaging method to 78 theoretical model combinations, using experimental Oslo data as a primary constraint. The results demonstrate that the theoretical uncertainty across the energy spectrum is significantly reduced. Among the tested ensembles, the D1M framework, particularly when accounting for temperature effects ($T = 0.5$ MeV), exhibits the highest consistency with experimental observations, followed by the microscopic EP+PDM at $T = 0.7$ MeV. Although further investigation is needed to clearly explain the temperature difference, the discrepancy in optimal temperatures reflects the different theoretical treatments of thermal damping in these frameworks. By prioritizing models based on their fit to empirical data, this work establishes a reliable, data-driven RSF baseline that reconciles divergent theoretical predictions.

Acknowledgement: *This work was funded by the National Foundation for Science and Technology Development (NAFOSTED) of Vietnam, Grant No. 103.04-2025.22.*

REFERENCES

[1]. G. A. Bartholomew, E. D. Earle, A. J. Ferguson, J. W. Knowles, M. A. Lone, *"Gamma-Ray Strength Functions"*, Advances in Nuclear Physics, pp. 229–324, (1973).

[2]. W. Hauser, H. Feshbach, *"The Inelastic Scattering of Neutrons"*, Physical Review, vol. 87, pp. 366–373, (1952).

[3]. J. Koning, S. Hilaire, M. C. Duijvestijn, *"TALYS-1.0"*, pp. 211–214, (2007).
[4]. T. Rauscher, F.-K. Thielemann, K.-L. Kratz, *"Nuclear Level Density and the Determination of Thermonuclear Rates for Astrophysics"*, Physical Review C, vol. 56, pp. 1613–1625, (1997).
[5]. T. Rauscher, F. Thielemann, *"Astrophysical Reaction Rates From Statistical Model Calculations"*, Atomic Data and Nuclear Data Tables, vol. 75, (2000).
[6]. G. Tian et al., *"Fast Neutron Induced Reaction Cross Sections on Natural Manganese and Tantalum"*, Applied Radiation and Isotopes, vol. 204, p. 111150, (2024).
[7]. G. Reffo, F. Fabbri, K. Wisshak, F. Käppeler, *"Fast Neutron Capture Cross Sections and Related Gamma-Ray Spectra of Niobium-93, Rhodium-103, and Tantalum-181"*, Nuclear Science and Engineering, vol. 80, pp. 630–647, (1982).
[8]. H. Miyahara et al., *"Gamma-Ray Emission Probabilities of Ta-182"*, Applied Radiation and Isotopes, vol. 49, pp. 1383–1386, (1998).
[9]. G. P. Glasgow, L. T. Dillman, *"The Specific Gamma-Ray Constant and Exposure Rate Constant of Ta-182"*, Medical Physics, vol. 9, pp. 250–253, (1982).
[10]. E. J. Hall, R. Oliver, B. J. Shepstone, *"Routine Dosimetry with Tantalum 182 and Iridium 192 Wires"*, Acta Radiologica Therapy Physics Biology, vol. 4, pp. 155–160, (1966).
[11]. J. N. Avila et al., *"Tungsten Isotopic Compositions in Stardust SiC Grains from the Murchison Meteorite: Constraints on the s-Process in the Hf–Ta–W–Re–Os Region"*, Astrophysical Journal, vol. 744, p. 49, (2011).
[12]. R. Bergère, H. Beil, A. Veyssière, *"Photoneutron Cross Sections of La, Tb, Ho and Ta"*, Nuclear Physics A, vol. 121, pp. 463–480, (1968).
[13]. Makinaga et al., *"Dipole Strength of Ta-181 for the Evaluation of the Ta-180 Stellar Neutron Capture Rate"*, Physical Review C, vol. 90, p. 044301, (2014).
[14]. H. Utsunomiya et al., *"Cross Section Measurements of the Ta-181(γ,n)Ta-182 Reaction Near Neutron Threshold and the p-Process Nucleosynthesis"*, Physical Review C, vol. 67, p. 015807, (2003).
[15]. R. G. Helmer, R. C. Greenwood, C. W. Reich, *"Level Structure of Ta-182"*, Nuclear Physics A, vol. 168, pp. 449–486, (1971).
[16]. M. L. Stelts, J. C. Browne, *"Gamma-Ray Spectra from Capture of 2-eV to 3-keV Neutrons by Ta-181"*, Physical Review C, vol. 16, pp. 574–587, (1977).
[17]. C. P. Brits et al., *"Nuclear Level Densities and Gamma-Ray Strength Functions of Ta-180, 181, 182"*, Physical Review C, vol. 99, p. 054330, (2019).
[18]. J. Kopecky, M. Uhl, *"Test of Gamma-Ray Strength Functions in Nuclear Reaction Model Calculations"*, Physical Review C, vol. 41, pp. 1941–1955, (1990).
[19]. P. Axel, *"Electric Dipole Ground-State Transition Width Strength Function and 7-MeV Photon Interactions"*, Physical Review, vol. 126, p. 671, (1962).
[20]. S. Goriely, E. Khan, M. Samyn, *"Microscopic HFB + QRPA Predictions of Dipole Strength for Astrophysics Applications"*, Nuclear Physics A, vol. 739, pp. 331–352, (2004).
[21]. S. Goriely, E. Khan, *"Large-Scale QRPA Calculation of E1-Strength and Its Impact on the Neutron Capture Cross Section"*, Nuclear Physics A, vol. 706, pp. 217–232, (2002).
[22]. S. Goriely, *"Radiative Neutron Captures by Neutron-Rich Nuclei and the r-Process Nucleosynthesis"*, Physics Letters B, vol. 436, pp. 10–18, (1998).
[23]. I. Daoutidis, S. Goriely, *"Large-Scale Continuum Random-Phase Approximation Predictions of Dipole Strength for Astrophysical Applications"*, Physical Review C, vol. 86, p. 034328, (2012).
[24]. E. Grosse, A. Junghans, R. Massarczyk, *"Breaking of Axial Symmetry in Excited Heavy Nuclei as Identified in Giant Dipole Resonance Data"*, The European Physical Journal A, vol. 53, (2017).
[25]. N. Nhu Le, S. Cristallo, D. Vescovi, L. Tan Phuc, N. Quang Hung, *"Maxwellian-Averaged Cross Section of Ta-181(n,γ) Reaction and Its Astrophysical Implications"*, Nuclear Physics A, vol. 1023, p. 122450, (2022).
[26]. S. Goriely, V. Plujko, *"Simple Empirical E1 and M1 Strength Functions for Practical Applications"*, Physical Review C, vol. 99, p. 014303, (2019).
[27]. S. Goriely et al., *"Gogny-HFB+QRPA Dipole Strength Function and Its Application to Radiative Nucleon Capture Cross Section"*, Physical Review C, vol. 98, p. 014327, (2018).
[28]. T. von Egidy, D. Bucurescu, *"Systematics of Nuclear Level Density Parameters"*, Physical Review C, vol. 72, p. 044311, (2005).

[29]. S. Goriely et al., *"Reference Database for Photon Strength Functions"*, The European Physical Journal A, vol. 55, p. 172, (2019).

TÓM TẮT

Đánh giá hàm lực bức xạ của ^{182}Ta thông qua phương pháp trung bình mô hình với trọng số dựa trên χ^2

Việc xác định hàm lực bức xạ (RSF) cho ^{182}Ta hiện đang gặp khó khăn do phạm vi thực nghiệm bị phân mảnh, dẫn đến những sai lệch đáng kể giữa các mô hình lý thuyết, đặc biệt là ở những vùng thiếu dữ liệu thực nghiệm. Nghiên cứu này giải quyết khoảng trống đó bằng cách đánh giá một tập hợp gồm 78 tổ hợp mô hình E1 và M1, sử dụng phương pháp trung bình trọng số χ^2 được ràng buộc bởi dữ liệu hàm lực tổng cộng từ phương pháp Oslo. Trong số các mô hình được đánh giá, mô hình Hartree-Fock-Bogoliubov kết hợp gần đúng pha ngẫu nhiên giả hạt với lực D1M Gogny thể hiện sự phù hợp tốt nhất với dữ liệu thực nghiệm. Theo sau đó là mô hình vi mô kết cặp chính xác kết hợp mô hình suy giảm phonon. Nhìn chung, kết quả của chúng tôi chứng minh rằng việc tính trọng số dựa trên dữ liệu thực tế này giúp giảm đáng kể phương sai lý thuyết.

Từ khoá: Hàm lực bức xạ; ^{182}Ta; Mô hình trọng số χ^2.